Check for updates

Novel anionic surfactant-modified chlorhexidine and its potent antimicrobial properties†

Zilma Pereira Muneeswaran, [ID] [a,c] Baran Teoman, [ID] [a,e] Yu Wang, [a,c]
Haroon Chaudhry, [a,c] Tatiana V. Brinzari, [a] Gaurav Verma, [f] Lomaani Ranasinghe, [g]
Kylie Ryan Kaler, [g] Xiaoyi Huang, [b] Xing He, [b] Belvin Thomas, [ID] [c] Shiyou Xu, [a]
Chi-Yuan Cheng, [a] Jeffrey M. Boyd, [ID] [g] Dailin Chen, [b] Zhigang Hao, [ID] [a]
Shengqian Ma, [ID] [f] Tewodros Asefa, [ID] [c,d] Long Pan [ID] *[a] and Viktor Dubovoy [ID] *[a]

Chlorhexidine dodecyl sulfate (CHX-DS) was synthesized and characterized *via* single-crystal X-ray diffraction (SC-XRD), ^{1}H nuclear magnetic resonance (NMR) spectroscopy, ^{1}H nuclear Overhauser effect spectroscopy (NOESY), and attenuated total reflectance Fourier-transform infrared spectroscopy (ATR-FTIR). The solid-state structure, comprising a 1:2 stoichiometric ratio of chlorhexidine cations $[C_{22}H_{30}Cl_2N_{10}]^{2+}$ to dodecyl sulfate anions $[C_{12}H_{25}SO_4]^-$, is the first report of chlorhexidine isolated with a surfactant. CHX-DS exhibits broad-spectrum antibacterial activity and demonstrates superior efficacy for reducing bacteria-generated volatile sulfur compounds (VSCs) as compared to chlorhexidine gluconate (CHG). The minimum inhibitory concentrations (MICs) of CHX-DS were 7.5, 2.5, 2.5, and 10 μM for *S. enterica*, *E. coli*, *S. aureus*, and *S. mutans*, respectively. Furthermore, MIC assays for *E. coli* and *S. mutans* demonstrate that CHX-DS and CHX exhibit a statistically significant efficacy enhancement in 2.5 μM treatment as compared to CHG. CHX-DS was incorporated into SBA-15, a mesoporous silica nanoparticle (MSN) framework, and its release was qualitatively measured *via* UV-vis in aqueous media, which suggests its potential as an advanced functional material for drug delivery applications.

1. Introduction

Chlorhexidine (CHX) was discovered in the 1950s as a chemical disinfectant and antiseptic with broad antimicrobial activity against a wide variety of bacteria and fungi.[1] Due to its potent antimicrobial efficacy at low concentrations and ease of synthesis, CHX is prevalent in the healthcare and pharmaceutical industries as a prophylactic or treatment for microbial infections as well as to promote wound healing.[2–7] CHX is ubiquitous in hospitals and medical settings to prevent infections associated with medical devices or surgeries as well as to treat gingivitis and other oral diseases.[2,8–12] For example, CHX is used in hospital baths and pre-surgery handwashing, and for the prevention of catheter-related bloodstream infections and other healthcare-associated infections.[13] CHX is also used in the hospital neonatal section to cleanse the neonatal cord and prevent staphylococcal infection.[14] Due to its widespread use in mitigating microbial infections, it was one of the drug candidates evaluated as a nasal and oral antiseptic to reduce the spread of SARS-CoV-2.[15] Although CHX did not prove to be effective against SARS-CoV-2, it has shown better efficacy against other viral and bacterial infections and remains the conventional disinfectant used in clinical settings.[3]

CHX demonstrates biocidal efficacy by disrupting the bacterial cell function *via* the coordination of the guanidinium group within the bacterial phospholipid cell membrane, causing membrane depolarization and leakage of cytosolic components.[16,17] It is evident that CHX is of high importance for combating bacteria; however, the crystallization of novel CHX complexes is challenging due to its poor water-solubility and bioavailability, and it is typically delivered as a gluconate

*^{a}Colgate-Palmolive Company, 909 River Road, Piscataway, New Jersey 08854, USA.
E-mail: vdubovoy@gmail.com*

*^{b}Colgate-Palmolive Company, 338 Qingnian Road, Economic Development Zone,
Guangzhou 510620, China*

*^{c}Department of Chemistry and Chemical Biology, Rutgers, The State University of
New Jersey, 610 Taylor Road, Piscataway, New Jersey 08854, USA*

*^{d}Department of Chemical and Biochemical Engineering, Rutgers, The State
University of New Jersey, 98 Brett Road, Piscataway, New Jersey 08854, USA*

*^{e}Otto H. York Department of Chemical and Materials Engineering, New Jersey
Institute of Technology, 323 Dr. Martin Luther King Jr Boulevard, Newark, New
Jersey 07102, USA*

*^{f}Department of Chemistry, University of North Texas, 1508 W. Mulberry Street,
Denton, Texas 76201, USA*

*^{g}Department of Biochemistry and Microbiology, Rutgers, The State University of New
Jersey, 76 Lipman Drive, New Brunswick, New Jersey 08901, USA*

†Electronic supplementary information (ESI) available: Additional figures and
further experimental details. CCDC 2272261. For ESI and crystallographic data
in CIF or other electronic format see DOI: https://doi.org/10.1039/d3dt02559d

salt (*i.e.*, CHG). To the best of our knowledge, there have only been six distinct crystal structures successfully elucidated thus far.[18] Previously, CHX crystal structures have been reported with three distinct calix[4]arenes: carboxylate (H_2CH_x) (CO_3)·$4H_2O$, sulfate (H_2CH_x)(SO_4)·$3H_2O$, and cyclamate (CHC).[19–21] More recently, CHX has been used as a template to functionalize mesoporous organosilica nanoparticles which possess equal antibacterial properties to free CHX.[22]

Previous work has demonstrated that SDS significantly reduces the *in vivo* antiplaque efficacy of CHX, but there is a lack of evidence for the mechanistic explanation of this phenomenon.[23] Controversial discussions amongst researchers have been ongoing for many years regarding the antibacterial efficacy of CHX in the presence of SDS, and whether SDS inhibits CHX efficacy; however, no crystal structure has been resolved to conclude the debate.[23–26] Evidence is provided herein that when complexed with dodecyl sulfate (DS), the resulting CHX-DS possesses equal antimicrobial activity and improved efficacy in reducing volatile sulfur compounds (VSC) as compared to CHG. This work was also inspired by a recent finding previously reported by our group of another ammonium compound, cetylpyridinium, complexed with tri-chlorostannate, which possessed antimicrobial properties and efficacy in VSC reduction.[27] Furthermore, our group reported functionalizing MSNs with benzalkonium chloride and its effectiveness as an antibacterial agent.[28] Similarly in this paper, MSNs were functionalized with CHX-DS and their potential for further enhancing the antibacterial properties of CHX has been demonstrated. This work paves the way for further in-depth studies to elucidate the mechanism of CHX antibacterial properties in the presence of SDS and other counterions to improve our understanding and ultimately improve our antimicrobial treatments involving cationic antibacterial agents. Furthermore, the current work demonstrates that CHX-DS may exhibit some advantages over the industry standard CHG in healthcare and pharmaceutical applications.

2. Experimental

Synthesis of CHX-DS

Reagent grade sodium dodecyl sulfate, chlorhexidine gluconate, and methanol were supplied by Sigma-Aldrich (St Louis, MO, USA), Sigma-Aldrich (St Louis, MO, USA), and J.T. Baker (Radnor, PA, USA), respectively. All reagents were used without further purification. SDS was dissolved in methanol (10 wt%) and combined with CHG (20 wt%) to yield a 2 : 1 molar ratio, respectively. A cloudy solution was obtained after stirring and the reaction was heated to 80 °C in a water bath under magnetic stirring for 15 min until the solution became clear. Crystals formed in the solution as the temperature was gradually decreased to room temperature. The resulting crystals were used for SC-XRD. The solution was further cooled in an ice bath and allowed to sit overnight. The crystals were collected by vacuum filtration, washed with copious amounts of water,

and left to dry completely. The crystals were ground with a mortar and pestle to produce a fine white powder of CHX-DS.

Synthesis of CHX-DS@SBA-15

Pluronic P123, hydrochloric acid (34 wt%), and tetraethyl orthosilicate (TEOS) were supplied by BASF (Ludwigshafen, Germany), J.T. Baker (Radnor, PA, USA), and Sigma-Aldrich (St Louis, MO), respectively. All materials were used as received without further purification. The synthesis of Santa Barbara Amorphous (SBA-15) mesoporous silica nanoparticles (MSNs) entailed combining 8.0 g of Pluronic P123, 208 mL of water, and 48 mL of hydrochloric acid (34 wt%) under stirring, yielding a homogeneous solution. Subsequently, 17.06 g of TEOS was added dropwise and stirred for 24 h at 40 °C, ultimately resulting in the formation of a white precipitate. The heterogeneous mixture was filtered, washed with copious amounts of deionized water, and dried overnight in a vacuum oven at 50 °C. Calcination of the synthesized SBA-15 was conducted in air at 550 °C for 6 h with 10 °C min^{-1} as the ramp rate.

The calcined SBA-15 was dried at 100 °C for 2 h in a vacuum oven. After drying, 2 g of SBA-15 was added to 200 g of CHG solution (10 wt%). The solution was stirred for 72 h in a 40 °C water bath. After 72 h, the solution was filtered, washed with copious amounts of deionized water, and dried in a vacuum oven at 50 °C overnight to yield SBA-15 loaded with CHX (*i.e.*, CHX@SBA-15). Subsequently, 1 g of the CHX@SBA-15 was added to 200 g of SDS solution (10 wt%) in methanol and stirred for 48 h at room temperature. After 48 h, the heterogeneous mixture was filtered, washed with copious amounts of deionized water, and dried in a vacuum oven at 50 °C to yield SBA-15 loaded with CHX-DS (*i.e.*, CHX-DS@SBA-15).

ATR-FTIR

Infrared spectra were collected using a Bruker Vertex 70 FTIR spectrometer (Bruker Optics, Billerica, MA) equipped with a GladiATR diamond ATR accessory (Pike Technologies, Madison, WI). The spectra were acquired at a resolution of 4 cm^{-1} in the 80–4000 cm^{-1} spectral range. All measurements were carried out at room temperature.

Single crystal X-ray diffraction

The X-ray diffraction data were collected using a Bruker D8 Venture PHOTON 100 CMOS system equipped with a Cu Kα INCOATEC ImuS micro-focus source (λ = 1.54178 Å). The data were collected at 100 K. Indexing was performed using APEX3 (difference vectors method). Data integration and reduction were performed using SaintPlus 6.01. Absorption correction was performed by a multi-scan method implemented in SADABS. The space group was determined using XPREP implemented in APEX3. The structure was solved using SHELXT (direct methods) and was refined using SHELXL-2017 (full-matrix least-squares on F^2) through the OLEX2 interface program.[29–32] All non-hydrogen atoms were refined anisotropically. Hydrogen atoms were placed in geometrically calculated

positions and were included in the refinement process using the riding model.

Volatile sulfur compound analysis

Methyl mercaptan, a representative molecule of volatile sulfur compounds (VSCs), was used as a marker for the quantitative measurement of mouth malodor by using a gas chromatography–flame photometry detection (GC-FPD). Sample preparation entailed the dissolution of the CHG, SDS, and CHX-DS powders in methanol to a final concentration of 0.01 wt%. Hydroxyapatite (HAP) disks were incubated with whole saliva to develop pellicles and subsequently treated with the prepared solutions. After rinsing, the treated disks were transferred to headspace vials and incubated with VSC solution to mimic mouth malodor VSC generation. Methyl mercaptan in the headspace was measured using GC-FPD.

Antimicrobial assays

To determine the minimum inhibitory concentration (MIC) of the antimicrobial compounds, *Escherichia coli* strain K-12, *Salmonella enterica* serovar typhimurium LT2 and *Staphylococcus aureus* USA300_LAC were grown overnight in 5 mL of Mueller Hinton in 20 mL capacity culture tubes at 37 °C with agitation.[33–35] *Streptococcus mutans* Clark (ATCC) was grown overnight in 15 mL of brain heart infusion in 20 mL capacity culture tubes statically at 37 °C. The optical density at 600 nm (OD_{600}) was adjusted to 0.1 in Mueller Hinton (*E. coli*, *S. enterica*, and *S. aureus*) and reinforced clostridial media (*S. mutans*). One-hundred µL of adjusted culture was subcultured into the wells of clear, polystyrene 96-well microtiter plates (Greiner Bio-One) containing 100 µL of Mueller Hinton (*E. coli*, *S. enterica*, and *S. aureus*) or reinforced clostridial medium (*S. mutans*) with the antimicrobial compounds. The antimicrobial compounds were prepared as 100 µM stocks in dimethyl sulfoxide and were then serially diluted to give the final concentrations. The amount of drug complex added did not alter bacterial growth. End-point minimum inhibitory concentrations (MICs) were determined for seven replicates. Control wells containing uninoculated media with antimicrobials were used to standardize the data. The microtiter plates were statically incubated with polystyrene lids (Greiner Bio-One) at 37 °C. The OD_{600} was measured after 20 hours (*E. coli*, *S. enterica*, and *S. aureus*) and after 48 hours (*S. mutans*) using a Varioskan Lux microplate reader (Thermo Scientific).

To assess cell viability using the resazurin, *E. coli* K-12, *S. enterica* serovar typhimurium, *S. aureus* USA300_LAC, and *S. mutans* Clark strains were prepared as described above for the MIC growth assays. One-hundred µL of cells was subcultured into black, polystyrene 96-well microtiter plates (Greiner Bio-One) with polystyrene lids (Greiner Bio-One) containing 100 µL of media containing the antimicrobial compounds. The microtiter plates were incubated for 20 hours statically at 37 °C. Subsequently, 100 µL of 0.1 mg mL^{-1} resazurin prepared in phosphate buffered saline (PBS), pH 7.4, was added to each well. The microtiter plates were further incubated at

37 °C for 75 minutes before fluorescence (excitation 560 nm, emission 590 nm) was measured using a Varioskan Lux microplate reader (Thermo Scientific).

^{1}H NMR and NOESY experiments

^{1}H NMR measurements were performed on 1 wt% samples in deuterated methanol (99.9% D, Cambridge Isotope Laboratories) solution. All NMR spectra were acquired on a Bruker Avance spectrometer (Bruker–Biospin, Billerica, MA, USA) with a 5 mm cryoprobe probe operating at 500.0 MHz for ^{1}H at 25 °C. For the NOESY experiment, two scans of 16 384 data points were acquired for each 128 t_1 increment with a spectral width of 3500 Hz in both frequency dimensions. The data were then imported to MestRec Nova and adjusted to 4096 × 4096 points with zero filling in F1 and truncating in F2 for covariance processing. The chemical shift is referenced to 0 using tetramethylsilane (TMS).

N$_2$ porosimetry analysis

The porosity and surface area of the samples were investigated by N$_2$ adsorption–desorption studies at 77 K using a Tristar-3000 instrument (Micromeritics, USA). Before each adsorption–desorption study, the sample was degassed for 8 h at 120 °C under N$_2$ gas flow to remove any possible guest molecule adsorbed on the sample's surfaces. The surface areas and pore size distributions of the materials were calculated using the Brunauer–Emmett–Teller (BET) method and the Barrett–Joyner–Halenda (BJH) method, respectively. The pore size and pore volume were determined from the desorption data using the BJH method.

Thermogravimetric analysis

Thermogravimetric analyses (TGA) of the materials were conducted with a PerkinElmer TGA7 instrument at a heating rate of 10 °C min^{-1} under an air atmosphere that was flowing at a rate of 20 mL min^{-1}.

Powder X-ray diffraction

Powder X-ray diffraction (PXRD) data were collected at room temperature using a Rigaku SmartLab θ–2θ diffractometer with copper radiation (Cu Kα = 1.5406 Å) and a secondary monochromator operating at 40 kV and 50 mA, whereby sample 2θ values were measured between 0.75° and 8° at 0.05° min^{-1} scan speed and a step size of 0.01°. The crystallite size was calculated using the Debye–Scherrer equation,[36] and the *d*-spacing was obtained using Bragg's Law:[37]

$$d = \frac{n\lambda}{2\sin(\theta)} \tag{1}$$

3. Results and discussion

## Structural and compositional characterization

The FTIR absorption spectrum of the CHX-DS crystal was measured and compared with the starting reagents (*i.e.*, SDS and CHG) (Fig. 1). Analysis of the CHX-DS infrared spectrum
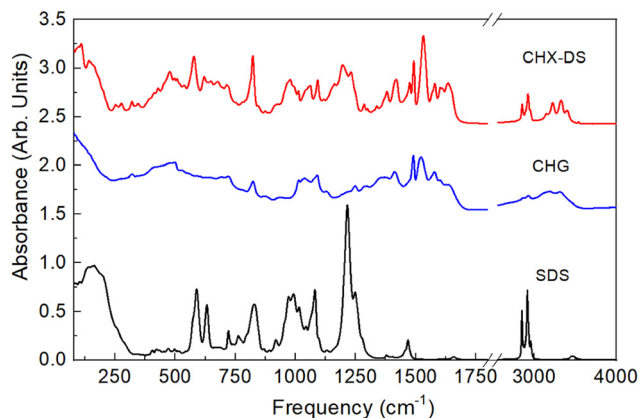
Fig. 1 Infrared absorption spectrum of a CHX-DS crystal in comparison with SDS and CHG reference compounds. The spectra are offset for clarity.

reveals the presence of both CHX and SDS components in the sample. For example, CHX bands corresponding to ν(C=C), ν(C=N), and δ(NH$_2$) vibrations are observed in the region above 1500 cm^{-1}, along with the N–H stretching modes of –NH, =NH, and NH$_2$ functional groups in the 3000–3500 cm^{-1} range.[38–40] Similarly, the SDS component can be identified from a prominent cluster of bands in the 1200–1275 cm^{-1} region associated with ν_{as}(SO$_2$) vibrations as well as intense $\nu_{as/sym}$(CH$_3$/CH$_2$) vibrations in the 2800–3000 cm^{-1} range.[41] Evidence of both CHX and SDS vibrational characteristics in the FTIR spectrum of the prepared crystal, combined with the fact that the absorption bands are significantly different in their shape and positions from the precursor materials, suggests the formation of the salt between chlorhexidine and sodium dodecyl sulfate ions.

To further confirm the formation of the CHX-DS complex, the crystal was dissolved in methanol and analyzed by NMR (Fig. S1–S2†) spectroscopy and MS (Fig. S3†). Additionally, SC-XRD analysis was carried out at 100 K showing that the coordination complex CHX-DS crystallizes in the triclinic $P1$ space group with the unit cell parameters a = 11.63(3) Å; b = 13.63(3) Å; c = 9.14(3) Å, and α = 70.24(10)°; β = 92.95(10)°; γ = 89.76(2)°. The structural formula can be described as [C$_{22}$H$_{32}$N$_{10}$Cl$_2$]·[(C$_{12}$H$_{25}$O$_4$S)$_2$] with the asymmetric unit consisting of one molecule of doubly protonated chlorhexidine cation and two molecules of dodecyl sulfate anion (Fig. 2). The
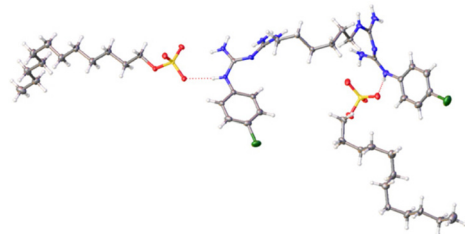
unit cell parameters and full crystallographic details are presented in Tables S1–S3.†

The structure comprises one CHX molecule surrounded by two DS molecules, whereby the biguanidine moieties of the CHX are symmetrically protonated by hydrogen transfer from the acidic sulfate group of the two DS molecules. These biguanidine moieties display a delocalization of the single and double bonds, as evident from the C–N bond lengths (1.313–1.357 Å), similar to other reported structures.[19–21] The CHX dications adopt a spiral conformation giving rise to U-shaped coils extending parallel to the a-axis (Fig. 3), similar to the (H$_2$CHX)(SO$_4$)·3H$_2$O structure reported by McCormick *et al.*, but different from the CHC structure previously reported by our group.[19,21] The CHX cations among the coils between the adjacent layers along the c-axis are anti to each other (Fig. S4†), giving rise to alternating layers of the CHX coils that are further involved in hydrogen bonding interactions to the sulfate anions of the DS molecules with one of the DS molecules being disordered (Fig. S5†).

Each of the CHX cations is involved in hydrogen bonding interactions with the sulfate groups from three different SDS molecules (Fig. 4). Two sulfate groups form two hydrogen bonds with the biguanide groups on the outer periphery, and one sulfate forms three hydrogen bonds with the inner –NH and –NH$_2$ groups of the biguanide moieties. The H-bonding ranges from 2.057 to 2.254 Å, indicating strong hydrogen bonding.[42] The PXRD pattern calculated from the single crystal structure also matches quite well with the one obtained from the bulk sample, indicating bulk phase purity (Fig. S6†).
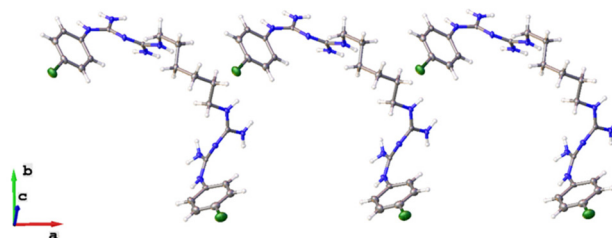
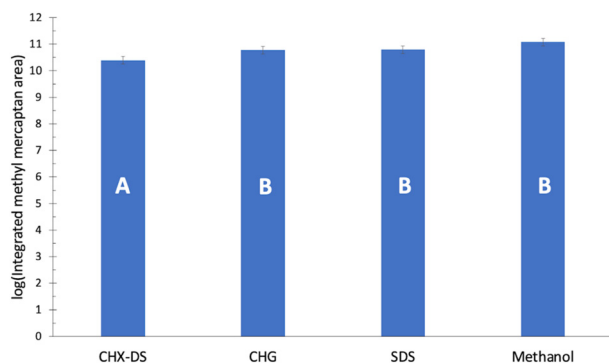**Fig. 3** The U-shaped conformation of the CHX cation extends along the a-axis.
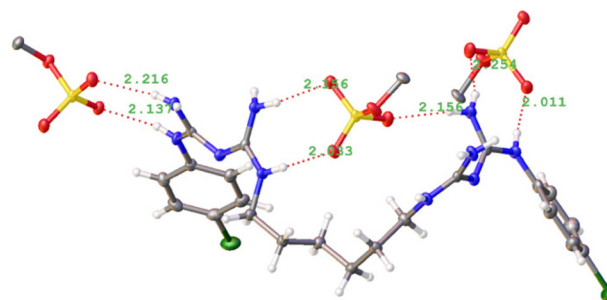
Fig. 4 The hydrogen bonding interactions between the CHX cation and the sulfate groups from three DS molecules.

Fig. 2 Structure of CHX complexing with two SDS units.
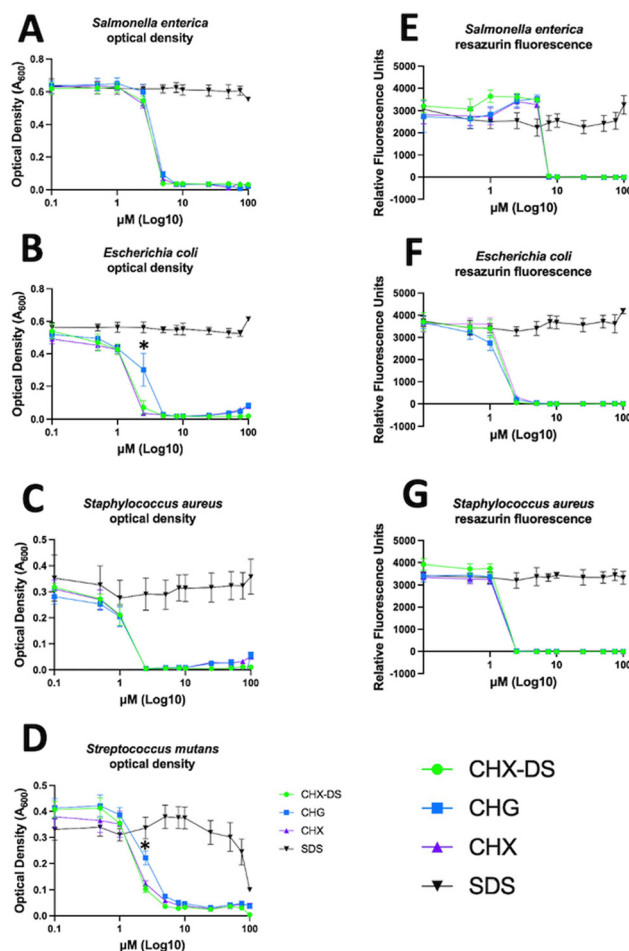
Volatile sulfur compound (VSC) reduction

Upon evaluating CHX-DS and its counterparts for *in vitro* bacteria-generated volatile sulfur compound reduction efficacy, it was determined that CHX-DS exhibits superior methyl mercaptan reduction efficacy as compared to the starting materials, including chlorhexidine gluconate, which is the current industry standard for a variety of biocidal applications. The differences between CHG, SDS, and methanol were not statistically significant (Fig. 5).

Antimicrobial assays

The antimicrobial activities of SDS, CHX, CHX-DS, and CHG were examined against both Gram-positive and Gram-negative bacteria (Fig. 6). Gram-negative *Salmonella enterica* serovar Typhimurium (panels 6A and 6E) causes salmonellosis globally.[43] The Gram-negative *Escherichia coli* strain K-12 (panels 6B and 6F) is non-pathogenic. Gram-positive *Staphylococcus aureus* (panels 6C and 6G) Los Angeles County (LAC) clone is a community-acquired methicillin-resistant *S. aureus* (MRSA) strain. Notoriously difficult to treat, MRSA infects the skin, lungs, and blood of people worldwide.[44] Gram-positive *Streptococcus mutans* (panel 6D) is the primary cause of dental caries.[45] CHX-DS, CHX, and CHG had a negative effect on the growth of all four bacterial strains. The minimal concentrations of CHX-DS necessary to fully inhibit the growth (MIC) of *S. enterica*, *E. coli*, *S. aureus*, and *S. mutans* were 7.5, 2.5, 2.5, and 10 μM, respectively. MIC assays for *E. coli* and *S. mutans* demonstrate that CHX-DS and CHX exhibit a statistically significant efficacy enhancement in the 2.5 μM treatment as compared to CHG. These results provide further evidence that the antimicrobial activity of CHX is not inhibited in the presence of anionic surfactants such as SDS, as proposed in the previous literature.[25] We also examined the effect of the compounds on viability and found that CHX, CHG, and CHX-DS decreased viability at similar concentrations. The minimal concentrations of CHX-DS necessary to prevent the viability of *S. enterica*, *E. coli*, and *S. aureus* were 7.5, 2.5, and 2.5 μM, respectively. Unfortunately, for unknown reasons, we were

Fig. 6 The effect of SDS (black inverted triangles), CHX (purple triangles), CHG (blue squares), and CHX-DS (green circle) on the growth (panels A, B, C, D) and viability (panels E, F, G) of *Escherichia coli*, *Salmonella enterica*, *Staphylococcus aureus*, and *Streptococcus mutans* is displayed. The data represent the average of seven independent cultures and the standard deviations are displayed for individual concentrations. Student's *t*-tests were performed on the 2.5 μM CHX, CHX-DS, and CHG samples and * indicates a *p* value <0.05.

unable to effectively measure the viability of *S. mutans* using the resazurin assay.

Synthesis of CHX-DS@SBA-15 and release studies

Previous reports demonstrated that antimicrobial molecules incorporated into MSNs exhibit enhanced antimicrobial activity as compared to the free molecule.[28] The stability of the structural framework, tunable pore size, high internal surface, and favorable biocompatibility allow for versatile applications in drug delivery and sustained drug release.[46,47] In this work, we explored the feasibility of incorporating CHX-DS into the SBA-15 framework for potential use as an advanced functional material with antimicrobial activity. SEM-EDX elemental analysis of CHX-DS@SBA-15 reveals concentrations of CHX and SDS of 2.85% and 0.90%, respectively (Fig. S7†). The TGA data are in good agreement with the SEM-EDX elemental analysis,

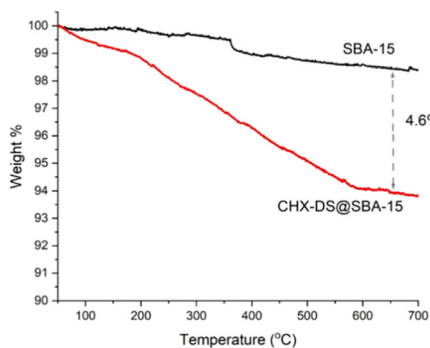

Fig. 5 VSC reduction efficacy is represented as methyl mercaptan concentration *via* gas chromatography. The mean of triplicate samples was plotted. The samples were grouped, denoted by A and B, using Tukey's method and 95% confidence level.

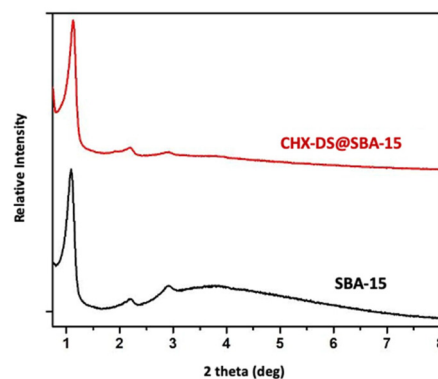**Fig. 7** TGA analysis of the as-synthesized SBA-15 and CHX-DS@SBA-15.

demonstrating a combined CHX and SDS content loading of approximately 4.60% (Fig. 7).

The surface area and porosity of the samples were investigated by collecting N_2 adsorption–desorption isotherms and applying the Brunauer–Emmett–Teller (BET) and Barrett–Joyner–Halenda (BJH) methods. The pore size and pore volume were determined from the desorption data using the BJH method with the results shown in Table 1 and Fig. 8.

The PXRD pattern of CHX-DS@SBA-15 exhibited two diffraction peaks at 2θ values of 1.14° and 2.22° corresponding to the (100) and (200) planes, respectively and an additional peak at the 2θ value of 2.92°.[48] These peaks correspond to the two-dimensional hexagonal structure of SBA-15 with highly ordered mesoporous channels. Significant differences in the PXRD pattern of CHX-DS@SBA-15 were not observed, indicating that the framework was intact throughout the loading of

Table 1 Surface area and porosity of synthesized materials

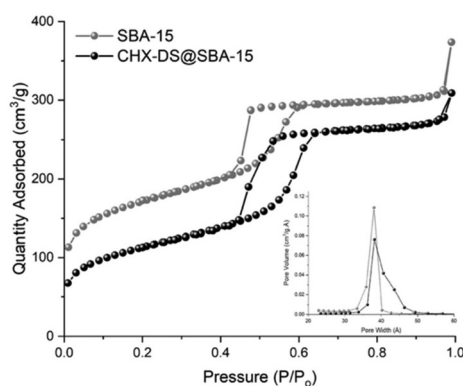| Materials	Surface area ($m^2\ g^{-1}$)	Pore size (nm)	Pore volume ($cm^3\ g^{-1}$)
SBA-15	572	4.8	0.50
CHX-DS@SBA-15	390	4.6	0.51

Fig. 8 Nitrogen (77 K) sorption isotherms of calcined SBA-15 and CHX-DS@SBA-15. Pore size distribution shown in the inset.

Fig. 9 The PXRD pattern of calcined SBA-15 and CHX-DS@SBA-15.

CHX-DS (Fig. 9). The *d*-spacing values, calculated using Bragg's Law, are shown in Table S7.†

Based on these analyses, we posit that a portion of the CHX and SDS speciation within CHX-DS@SBA-15 exists as CHX-DS; however, there is an excess of CHX which can be either singly or doubly electrostatically bound to the anionic silica surface or as a free molecule. Therefore, direct evidence of CHX-DS material was not attainable with the analysis techniques. Surface elemental analysis, measured using X-ray photoelectron spectroscopy (XPS), did not detect significant amounts of CHX or SDS on the surface of CHX-DS@SBA-15, suggesting that they predominantly diffused deeper into the SBA-15 pore framework instead of building up on the surface.

Although we were not able to quantify the amount of CHX-DS released from the as-synthesized CHX-DS@SBA-15, the presence of soluble chlorhexidine was detected in the supernatant of a mixture comprising 100 mg of CHX-DS@SBA-15 in 50 mL of acidic (pH 4.0) and neutral (pH 7.0) aqueous environments. UV-vis analysis (not shown) on the supernatant revealed absorbance peaks at λ_{max} of 231 and 260 nm, which is consistent with literature-reported values for CHX.[49] Broad interference peaks were observed in the UV-vis spectrum, presumably due to the presence of silica nanoparticles. Nevertheless, the presence of chlorhexidine in the supernatant indicates its release from CHX-DS@SBA-15 which supports its potential use as an advanced functional material for drug delivery applications.[22,28]

4. Conclusions

In this work, a novel solid-state structure comprising CHX and SDS was synthesized, the crystal structure was elucidated, and it was used in the synthesis of advanced functional materials with potential for drug delivery system applications. The novel CHX-DS complex exhibits antimicrobial activity against four bacteria: *S. aureus* LAC, *S. enterica* serovar Typhimurium, *S. mutans* and *E. coli* K-12, providing evidence in contrast to previous literature which claimed that SDS inhibits CHX efficacy. The single-crystal structure elucidation revealed that

CHX-DS consists of one chlorhexidine molecule and two dodecyl sulfate molecules. Volatile sulfur compound data demonstrated that CHX-DS is more effective than CHG in reducing volatile sulfur compounds generated by bacteria. Furthermore, CHX-DS was loaded onto mesoporous silica and its release in aqueous media was confirmed indicating its potential application in drug delivery systems. This work paves the way for further in-depth investigations into the anti-microbial activity of quaternary ammonium compounds (QACs) and bisbiguanides in the presence of anionic (surfactant) molecules.

Author contributions

Zilma Pereira Muneeswaran and Baran Teoman are co-authors of this manuscript as both contributed equally to the formal analysis, investigation, conceptualization, and completion of this research work. The co-authors and their contribution to the work are as follows: Yu Wang contributed to the initial synthesis of the complex. Haroon Chaudhry performed mesoporous silica loading synthesis and experiments. Tatiana V. Brinzari performed all ATR-FTIR analyses, Gaurav Verma and Shengqian Ma collected and solved XRD data. Lomaani Ranasinghe, Kylie Ryan Kaler, and Jeffrey M. Boyd analysed antimicrobial activity. Xiaoyi Huang, Xing He, and Dailin Chen analysed VSC inhibition. Belvin Thomas and Tewodros Asefa performed the BET and BJH experiments. Chi-Yuan Cheng, Zhigang Hao, and Shiyou Xu collected NMR spectroscopy, MS, and other analytical data, respectively. Long Pan and Viktor Dubovoy are the corresponding authors as they were responsible for leading and overseeing all research activity, planning, and execution of experiments. All authors wrote and edited the manuscript.

Conflicts of interest

There are no conflicts to declare.

Acknowledgements

References

1 G. McDonnell and A. D. Russell, *Clin. Microbiol. Rev.*, 1999, **12**(1), 147.

2 K. S. Lim and P. C. Kam, *Anaesth., Pain Intensive Care*, 2008, **36**, 502.

3 M. D. S. Fernandez, M. I. F. Guedes, G. P. J. Langa, C. K. Rösing, J. Cavagni and F. Muniz, *Odontology*, 2022, **110**, 376.

4 Y. Shi, N. Yang, L. Zhang, M. Zhang, H. H. Pei and H. Wang, *Am. J. Infect. Control*, 2019, **47**, 1255.

5 G. P. Privitera, A. L. Costa, S. Brusaferro, P. Chirletti, P. Crosasso, G. Massimetti, A. Nespoli, N. Petrosillo, M. Pittiruti, G. Scoppettuolo, F. Tumietto and P. Viale, *Am. J. Infect. Control*, 2017, **45**, 180.

6 T. M. Karpiński and A. K. Szkaradkiewicz, *Eur. Rev. Med. Pharmacol. Sci.*, 2015, **19**, 1321.

7 A. Pilloni, S. Ceccarelli, D. Bosco, G. Gerini, C. Marchese, L. Marini and M. A. Rojas, *Antibiotics*, 2021, **10**(10), 1192.

8 D. A. Van Strydonck, D. E. Slot, U. Van der Velden and F. Van der Weijden, *J. Clin. Periodontol.*, 2012, **39**, 1042.

9 M. Addy, S. Jenkins and R. Newcombe, *J. Clin. Periodontol.*, 1990, **17**, 693.

10 D. A. Van Strydonck, S. Scalé, M. F. Timmerman, U. Van der Velden and G. A. Van der Weijden, *J. Clin. Periodontol.*, 2004, **31**, 219.

11 J. Kolahi and A. Soolari, *Quintessence Int.*, 2006, **37**, 605.

12 C. G. Emilson, *J. Dent. Res.*, 1994, **73**, 682.

13 A. Babiker, J. D. Lutgring, S. Fridkin and M. K. Hayden, *Clin. Infect. Dis.*, 2021, **72**, 891.

14 Chlorhexidine, in *Meyler's Side Effects of Drugs*, ed. J. K. Aronson, Elsevier, Oxford, 16th edn, 2016, pp. 239–248.

15 C. Stathis, N. Victoria, K. Loomis, S. A. Nguyen, M. Eggers, E. Septimus and N. Safdar, *Future Microbiol.*, 2021, **16**, 119.

16 P. Maris, *Rev. Sci. Tech.*, 1995, **14**, 47.

17 P. Gilbert and L. E. Moore, *J. Appl. Microbiol.*, 2005, **99**, 703.

18 F. Sarmiento, J. M. del Rio, G. Prieto, D. Attwood, M. N. Jones and V. Mosquera, *J. Phys. Chem.*, 1995, **99**, 17628.

19 D. Cattaneo, L. J. McCormick, D. B. Cordes, A. M. Slawin and R. E. Morris, *J. Mol. Struct.*, 2016, **1121**, 70.

20 N. Dupont, A. N. Lazar, F. Perret, O. Danylyuk, K. Suwinska, A. Navaza and A. W. Coleman, *CrystEngComm*, 2008, **10**, 975.

21 V. Dubovoy, P. Desai, Z. Hao, C. Y. Cheng, G. Verma, L. Wojtas, T. V. Brinzari, J. M. Boyd, S. Ma, T. Asefa and L. Pan, *Cryst. Growth Des.*, 2020, **20**, 4991.

22 Y. He, Y. Zhang, M. Sun, C. Yang, X. Zheng, C. Shi, Z. Chang, Z. Wang, J. Chen, S. Pei, W. F. Dong, D. Shao and J. She, *Colloids Surf., B*, 2020, **187**, 110653.

23 P. Barkvoll, G. Rølla and K. Svendsen, *J. Clin. Periodontol.*, 1989, **16**, 593.

24 T. A. Elkerbout, D. E. Slot, E. W. Bakker and G. A. Van der Weijden, *Int. J. Dent. Hyg.*, 2016, **14**, 42.

25 P. Bonesvoll, *Arch. Oral Biol.*, 1977, **22**, 273.

26 D. A. Van Strydonck, M. F. Timmerman, U. Van der Velden and G. A. Van der Weijden, *J. Clin. Periodontol.*, 2006, **33**, 340.

27 B. Teoman, Z. P. Muneeswaran, G. Verma, D. Chen, T. V. Brinzari, A. Almeda-Ahmadi, J. Norambuena, S. Xu,

S. Ma, J. M. Boyd, P. M. Armenante, A. Potanin, L. Pan, T. Asefa and V. Dubovoy, *ACS Omega*, 2021, **6**(51), 35455.

28 V. Dubovoy, A. Ganti, T. Zhang, H. Al-Tameemi, J. D. Cerezo, J. M. Boyd and T. Asefa, *J. Am. Chem. Soc.*, 2018, **140**(42), 13534.

29 G. M. Sheldrick, *Acta Crystallogr., Sect. A: Found. Crystallogr.*, 1990, **46**, 467.

30 G. M. Sheldrick, *Acta Crystallogr., Sect. A: Found. Crystallogr.*, 2008, **64**, 112.

31 G. M. Sheldrick, *Acta Crystallogr., Sect. C: Struct. Chem.*, 2015, **71**, 3.

32 O. V. Dolomanov, L. J. Bourhis, R. J. Gildea, J. A. K. Howard and H. Puschmann, *J. Appl. Crystallogr.*, 2009, **42**, 339.

33 F. R. Blattnet, G. Plunkett, C. A. Bloch, N. T. Perna, V. Burland, M. Riley, J. Collado-Vides, J. D. Glasner, C. K. Rode, G. F. Mayhew, J. Gregor, N. W. Davis, H. A. Kirkpatrick, M. A. Goeden, D. J. Rose, B. Mau and Y. Shao, *Science*, 1997, **277**(5331), 1453.

34 J. M. Boyd, W. P. Teoh and D. M. Downs, *J. Bacteriol.*, 2012, **194**(3), 576.

35 J. S. Patel, J. Norambuena, H. Al-Tameeni, Y. M. Ahn, A. L. Perryman, X. Wang, S. S. Daher, J. Occi, R. Russo, S. Park, M. Zimmerman, H. P. Ho, D. S. Perlin, V. Dartois, S. Ekins, P. Kumar, N. Conell, J. M. Boyd and J. S. Freundlich, *ACS Infect. Dis.*, 2021, **7**(8), 2508.

36 U. Holzwarth and N. Gibson, *Nat. Nanotechnol.*, 2011, **6**, 534.

37 B. Cantor, *The Equations of Materials*, Oxford University Press, Oxford, 2020.

38 M. F. Călinescu, T. Negreanu-Pîrjol, R. Georgescu and O. Călinescu, *Cent. Eur. J. Chem.*, 2010, **8**, 543.

39 D. Luo, S. Shahid, R. M. Wilson, M. J. Cattell and G. B. Sukhorukov, *ACS Appl. Mater. Interfaces*, 2016, **8**, 12652.

40 T. Rema, J. R. Lawrence, J. J. Dynes, A. P. Hitchcock and D. R. Korber, *Antimicrob. Agents Chemother.*, 2014, **58**, 5673.

41 R. B. Viana, A. B. F. da Silva and A. S. Pimentel, *Adv. Phys. Chem.*, 2012, **14**, 903272.

42 G. A. Jeffrey, *An Introduction to Hydrogen Bonding*, OUP, 1997.

43 A. Fabrega and J. Vila, *Clin. Microbiol. Rev.*, 2013, **26**(2), 308.

44 P. J. Planet, *J. Infect. Dis.*, 2017, **215**, S71.

45 W. J. Loesche, *Microbiol. Rev.*, 1986, **50**(4), 353.

46 H. Yan, S. Wang, L. Han, W. Peng, L. Yi, R. Guo, S. Liu, H. Yang and C. Huang, *J. Dent.*, 2018, **78**, 83.

47 T. Asefa and V. Dubovoy, in *Comprehensive Supramolecular Chemistry II*, ed. J. L. Atwood, Elsevier, Oxford, 2017, pp. 157.

48 F. Hassanzadeh-Afruzi, S. Asgharnasl, S. Mehraeen, Z. Amiri-Khamakani and A. Maleki, *Sci. Rep.*, 2021, **11**, 19852.

49 P. F. Gan, M. Sahidin, A. Aziz and C. Ngui, *Malays. J. Sci.*, 2011, **30**(3), 171–176.